applied sciences

MDPI

Article

Effects of Amyloid Beta (Aβ) Oligomers on Blood–Brain Barrier Using a 3D Microfluidic Vasculature-on-a-Chip Model

Samuel Chidiebere Uzoechi [1,2], Boyce Edwin Collins [1], Cody Joseph Badeaux [1], Yan Li [3], Sang Su Kwak [4], Doo Yeon Kim [4], Daniel Todd Laskowitz [5], Jin-Moo Lee [6] and Yeoheung Yun [1,*]

[1] Department of Chemical, Biological, and Bioengineering, North Carolina Agricultural and Technical State University, Greensboro, NC 27411, USA; scuzoechi@ncat.edu (S.C.U.); becollin@ncat.edu (B.E.C.); cjbadeaux@aggies.ncat.edu (C.J.B.)
[2] Department of Biomedical Engineering, Federal University of Technology, PMB 1526, Owerri 460114, Nigeria
[3] Chemical & Biomedical Engineering, College of Engineering, Florida State University, Tallahassee, FL 32310, USA; yli@eng.famu.fsu.edu
[4] Genetics and Aging Research Unit, Mass General Hospital, Harvard Medical School, 114 16th Street, Charlestown, MA 02129, USA; sskwak@mgh.harvard.edu (S.S.K.); dykim@mgh.harvard.edu (D.Y.K.)
[5] Neurosurgery, Anesthesiology & Neurobiology, Duke University Medical Center, Durham, NC 27710, USA; daniel.laskowitz@duke.edu
[6] Department of Neurology, Washington University School of Medicine, St. Louis, MO 63110, USA; leejm@wustl.edu
* Correspondence: yyun@ncat.edu; Tel.: +1-(336)-285-3226

Abstract: The disruption of the blood–brain barrier (BBB) in Alzheimer's Disease (AD) is largely influenced by amyloid beta (Aβ). In this study, we developed a high-throughput microfluidic BBB model devoid of a physical membrane, featuring endothelial cells interacting with an extracellular matrix (ECM). This paper focuses on the impact of varying concentrations of $A\beta_{1–42}$ oligomers on BBB dysfunction by treating them in the luminal. Our findings reveal a pronounced accumulation of $A\beta_{1–42}$ oligomers at the BBB, resulting in the disruption of tight junctions and subsequent leakage evidenced by a barrier integrity assay. Additionally, cytotoxicity assessments indicate a concentration-dependent increase in cell death in response to $A\beta_{1–42}$ oligomers (LC50 ~ 1 μM). This study underscores the utility of our membrane-free vascular chip in elucidating the dysfunction induced by Aβ with respect to the BBB.

Keywords: blood–brain barrier; microfluidic; amyloid beta; Alzheimer's Disease (AD)

Citation: Uzoechi, S.C.; Collins, B.E.; Badeaux, C.J.; Li, Y.; Kwak, S.S.; Kim, D.Y.; Laskowitz, D.T.; Lee, J.-M.; Yun, Y. Effects of Amyloid Beta (Aβ) Oligomers on Blood–Brain Barrier Using a 3D Microfluidic Vasculature-on-a-Chip Model. *Appl. Sci.* **2024**, *14*, 3917. https://doi.org/10.3390/app14093917

Academic Editor: Eric Chappel

Received: 14 March 2024
Revised: 25 April 2024
Accepted: 29 April 2024
Published: 4 May 2024

1. Introduction

The blood–brain barrier (BBB) is necessary for normal brain function and maintains the central nervous system (CNS) homeostatic environment. Specialized endothelial cells and supporting cells such as neurons, oligodendrocytes, microglia, astrocytes, and pericytes make up the blood–brain barrier (BBB) [1,2]. Adherens junctions and tight junctions, along with a few other unique transport mechanisms, allow the blood–brain barrier (BBB) to regulate the entry of substances into the brain [3,4]. The BBB's barrier qualities, however, also make it more difficult to treat CNS illnesses, since they prevent many large- and small-molecule medications from getting into the brain in amounts sufficient to cause a therapeutic reaction [5]. With respect to Alzheimer's disease (AD), studies show that $A\beta_{1–42}$ plays a central role in Aβ accumulation and plaque formation in the brain [6,7]. The blood–brain barrier (BBB) plays a crucial role in the regulation of Aβ levels in the brain, and its dysfunction is closely related to the accumulation of Aβ caused by Alzheimer's disease (AD) [6,7]. Understanding vascular contributions to cognitive impairment and dementia (VCID) is significant due to the cognitive decline resulting from damage to the brain function [8]. Another aspect of AD-related emerging issues is cerebral amyloid angiopathy (CAA). CAA is a type of cerebrovascular disorder characterized by the accumulation of Aβ

within the leptomeninges and small-to-medium-sized cerebral blood vessels [9]. CAA is associated with cognitive dysfunction, intracerebral hemorrhage (ICH), and microinfarcts. CAA is tightly linked with FDA-approved anti-Aβ immunotherapy as a side effect [10]. The main receptors for Aβ transport across the BBB from brain to blood and blood to brain are low-density lipoprotein receptor-related protein-1 (LRP1) and receptor for advanced glycation end products (RAGE), respectively [11,12]. Tight junction (TJ) proteins such as ZO-1, claudin-5, and occludin are part of the components of the BBB and are considered, in part, important indicators of the morphological changes in the BBB [13]. Apart from the molecular basis of AD, this model can be used to model other neurological disorders and neurodegenerative diseases [14].

Although whole-organism drug distribution can be studied using in vivo models, their use for BBB-penetrant antibody screening is limited due to the intricacy of this process and the reduced throughput of these investigations. Because of this, the field's in vivo research is supplemented with quicker and easier in vitro models, such as the transwell technique [15–17] and several on-a-chip technologies [18–20]. Even though in vitro BBB modeling has advanced significantly in recent years, a model that combines physiologically appropriate circumstances such as flow, coculture, and the absence of artificial membranes with quick, high-throughput readouts is still required. To address some of the key limitations of the current models, we generated a 3D bioengineered microfluidic membrane-free BBB against ECM using a phase guide method, a geometric feature that acts as a pressure barrier due to meniscus pinning. Here, we studied Aβ trafficking through the BBB using the two-lane perfusion-based microfluidic device. This perfusion-based microfluidic device would offer numerous advantages, including reproducibility, reduced sample volumes and cost, precise control of media flow and reagent delivery, and the ability to regulate the spatiotemporal parameters of the brain microenvironment.

2. Materials and Methods

2.1. Cell Culture

Primary human umbilical vein endothelial cells (HUVECs-C2519AS) were purchased from Lonza (Basel, Switzerland) [21]. Endothelial cells were expanded in T-75 flasks (Nunc™ EasyFlask, Sigma F7552 (Sigma-Aldrich, St. Louis, MI, USA)) and used for four-to-six passages and cultured in endothelial cell growth medium-2 (EGM™-2) and BulletKit™ (Lonza, Basel, Switzerland, CC-3162), with media change occurring every 3 days [22]. All cells were cultured in a humidified incubator at 37 °C and 5% CO_2 to allow for optimal cell growth and differentiation.

2.2. Microfluidic Cell Culture

The membrane-free blood–brain barrier (BBB) was constructed using a microfluidic device. A two-lane microfluidic OrganoPlate with 96 vascular channels and with dimensions 400 µm × 220 µm (w × h) and a phase guide of dimensions 100 µm × 55 µm (w × h) (MIMETAS BV, Gaithersburg, MD, USA) were used to engineer the BBB-like construct [23]. Figure 1 shows the process of BBB tissue construction. The channels were injected with 2 µL of extracellular matrix (ECM) prepared at the ratio of 8:1:1 of type I (Corning, Collagen I Rat Tail, 9.48 mg/mL), 1 M HEPES (ThermoFisher, Norristown, PA, USA, 15630-080), and 37 g/L $NaHCO_3$, and the OrganoPlate was incubated for 15 min at 37 °C and 5% CO_2 to allow for ECM to polymerize [23]. To prevent the polymerized ECM from drying out, 50 µL of HBSS (ThermoFisher, 14175-079) was added to the gel inlet. Subsequently, p4 endothelial cells were harvested with TrypLE™ Express (ThermoFisher, 12605010). HUVECs were seeded in microfluidics at the density of 10,000 cells/µL. A total of 2 µL of endothelial cell suspension was seeded in the medium inlet (perfusion channel or blood lane), 50 µL of endothelial cell complete media was added to the top medium inlet, and HBSS was aspirated from the gel inlet. The plate was incubated at its side in the plate stand for 6 h to allow the cells on the top channel to settle against the ECM and attach [23,24]. Afterward, 50 µL of endothelial cell complete media was added to the perfusion media outlet and

placed on the interval rocker switching between a +7° and a −7° angle of inclination every 8 min, enabling bidirectional fluid flow [23]. The cells were cultured for 5 days at 37 °C and 5% CO_2 to form BBB against ECM before being treated with $A\beta_{1–42}$ at different concentrations. The endothelial cell medium on both perfusion inlet and outlet was refreshed every two days with 50 µL each.

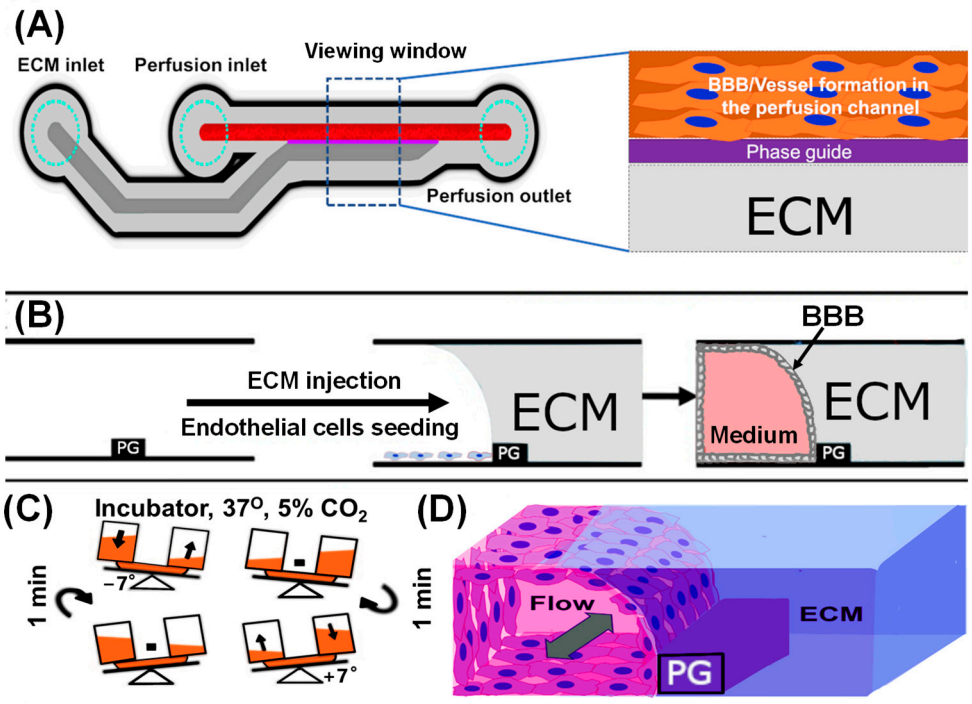

Figure 1. The schematic diagram for the construction of the 3D BBB system in the microfluidic device. (**A**) The schematic structure of a microfluidic chip and the representative design depicting the observation window. (**B**) Experimental procedure for the construction of a 3D neurovascular/brain compartment. (**C**) The incubation of a microfluidic device in a dynamic perfusion that allows bidirectional fluid flow. (**D**) Schematic illustration of the expected 3D reconstruction of the endothelial-cell-based vascular barrier (tunable perfusion).

2.3. Amyloid Beta 1–42 ($A\beta_{1–42}$) Oligomer Preparation and Treatment

Biotinyl–Amyloid β Protein ($A\beta_{1–42}$) was purchased (Bachem, Bubendorf, Switzerland, 4038795) and stored in desiccated containers at −80 °C. Before use, the peptide was allowed to equilibrate to room temperature for at least 30 min to avoid condensation upon opening the vial [25]. A 1 mM of Biotinyl–Amyloid β Protein ($A\beta_{1–42}$) treatment solution was prepared in the fume hood by dissolving 0.5 mg of $A\beta_{1–42}$ in 105.5 µL of 100% 1,1,1,3,3,3-Hexafluoro-2-propanol (HFIP) (ThermoFisher, 147541000) [25,26]. The clear solution containing 1 mM of dissolved $A\beta_{1–42}$ was then aliquoted in 0.6 µL low-retention microcentrifuge tubes (ThermoFisher, 3449). The samples were left in the fume hood overnight to allow HFIP to evaporate and were left 1 h in the desiccator to promote evaporation of any remaining HFIP. Then, the subsequent clear $A\beta_{1–42}$ film was resuspended in sterile DMSO (Sigma-Aldrich, 08418) by gently scraping up and down until the peptide film was completely dissolved [26]. The peptide solution was mildly vortexed for 30 s, followed by 5 min of sonication in an ultrasonic bath cleaner (Branson 2510). Twenty-four hours before treatment, $A\beta_{1–42}$ solutions were diluted in EGM-2 medium to the final concentrations of 10 µM, 20 µM, and 30 µM, respectively. A 5-day culture of endothelial cells in the microfluidic device was treated with $A\beta_{1–42}$ solutions for 48 h. The following design was used throughout the experiments: (1) BBB-No Aβ (BBB without Aβ), (2) ECM Only + 20 µM (Aβ without BBB), and (3) 10 µM, 20 µM, and 30 µM (Aβ with BBB). It is important to note that ECM was injected into the gel channel in all conditions.

2.4. Barrier Integrity Assay

The barrier integrity assay was performed to measure the barrier function and lumen formation of endothelial vessels grown in the microfluidic device. Perfusion channels were washed once for 5 min with 25 µL EGM-2 complete media to confirm the appropriate flow profile during successive barrier integrity assays [23]. Afterward, all media were aspirated from the chips. A fluorescein isothiocyanate FITC-dextran (MW: 40 kDa; Chondrex) solution was made by dissolving 0.5 mg/mL solution in complete EGM-2 media. Then, 20 µL of EGM-2 media without fluorescent dye was added to the gel inlet (basal side of the chip). A total of 40 µL and 30 µL of FITC solution was added to the media inlet and outlet which contained endothelial microvessels, and the image acquisition was started. Image acquisition was performed on an EVOS M5000 multichannel fluorescence microscope coupled with a stage incubator using the time-lapse function (10-min, 20-s intervals). The apparent permeability was quantified using ImageJ (Version 1.54i, March 2024) [27]. Data were plotted using GraphPad Prism 8.0 (GraphPad Software, San Diego, CA, USA). We used the following formula to get the apparent permeability (P_{app}) value [28]:

$$P_{app} = \frac{\Delta C_{receiver} \times V_{receiver}}{\Delta t \times A_{barrier} \times C_{donor}} \left(\frac{\text{cm}}{\text{s}}\right)$$

The fluorescence intensity measured in the ECM channel between t = 0 and t = 10 min is represented by $\Delta C_{receiver}$. The volume of the measured region in the ECM channel (h × w × l) is represented by $V_{receiver}$. Δt is the duration between start and finish (10 min). The surface of the ECM interface with the medium channel is represented by $A_{barrier}$, and the fluorescence intensity measured in the top perfusion channel is represented by C_{donor}. This formula assumes that the curve is linear, often maintained when the receiver's concentration is less than 10% of the donor's [28].

2.5. Immunocytochemistry

Unless otherwise stated, all steps were performed at room temperature on a rocking platform. Briefly, a 3D microfluidic model of the endothelial cell was fixed with 4% PFA (ThermoFisher, J19943-K2) for 15 min, followed by permeabilization with 0.3% Triton X-100 (ThermoFisher, EP151-100) in PBS for 10 min. Then the samples were washed with 4% FBS (Atlanta Biological, Flowery Branch, GA, USA, S11050) in PBS for 5 min. Afterward, the samples were blocked with 2% FBS (Atlanta Biological, S11050), 2% BSA (Sigma-Aldrich, AB412), and 0.1% Tween 20 (Sigma Aldrich, P9416) in PBS (1× Corning, Corning, NY, USA, 21-040-CV) for 45 min. Respectively, 10 µL of solution of Streptavidin conjugated to secondary antibody at 1:100 (AF 594, Invitrogen, Carlsbad, CA, USA, S11227) and ZO-1 conjugated to secondary antibody at 1:100 (AF488; Invitrogen, 339188) were added to the media inlet and outlet and incubated overnight at 4 °C on a rocking platform. Afterward, the plate was washed and 20 µL of Hoechst 1:500 (Invitrogen, Waltham, MA, USA, H3570) was added to the media inlet and outlet overnight. Data were acquired and processed using a two-photon confocal microscope (ZEISS Multiphoton LSM 710) equipped with ZEN Blue software (Version 3.6, Carl Zeiss Microscopy GmbH, Oberkochen, Germany).

2.6. Cell Viability Assay

First, the culture medium was aspirated, and the cells were washed with PBS (1X Corning, 21-040-CV; 50 µL for inlet and outlet, respectively) on a rocker. Cell viability was determined by staining the channels with a two-probe solution containing 4 mM of ethidium homodimer-1 (EthD-1, Invitrogen, E1169) in PBS and 2.4 mM of calcein AM (Invitrogen, L3224) [21]. A total of 50 µL and 10 µL of the stain solution were added to the perfusion/media inlet and outlet and rocked for 30 min. The channels were washed with PBS for 1 min while rocking (50 µL into the media inlet and outlet, respectively). A total of 50 µL of PBS was added to the inlets and outlets, and the samples were imaged using ImageXpress Micro Confocal (Molecular Devices).

2.7. Statistical Analysis

Statistical analyses were performed using Prism GraphPad software (version 8.0, GraphPad Software, San Diego, CA, USA). Descriptive statistics such as mean, standard deviation, and frequency were calculated for all variables of interest. One-way analysis of Variance (ANOVA) was conducted as appropriate. Statistical significance was considered at a 99.9% confidence interval ($p < 0.001$) unless otherwise stated. The results of the statistical analyses are reported with appropriate measures of effect size and confidence intervals. Perfusion rates were quantified by analyzing images with ImageJ software.

3. Results

3.1. Microfluidic 3D BBB-on-a-Chip

Figure 2A shows bright-field images of the BBB tissue construction process with (1) ECM injection, (2) endothelial cells (ECs) seeding against ECM, and (3) membrane-free BBB formation. Using capillary pressure barriers known as phase guides, we first loaded the ECM into the brain lane (or ECM channel) and allowed the ECM to polymerize in the incubator [21]. The endothelial cells were seeded on the blood lane (or perfusion channel) against the ECM on the brain lane (Figure 2A). In 5–7 days, endothelial cells created a confluent monolayer after adhering steadily to the ECM, and then they produced a tubular structure (Figure 2B). A perfusion rocker was used to maintain the plate shear stress and fluidic flow (Figure 1C). The final BBB tissue construct was used for different functional assays, including barrier integrity, amyloid beta trafficking, migration, and cell viability.

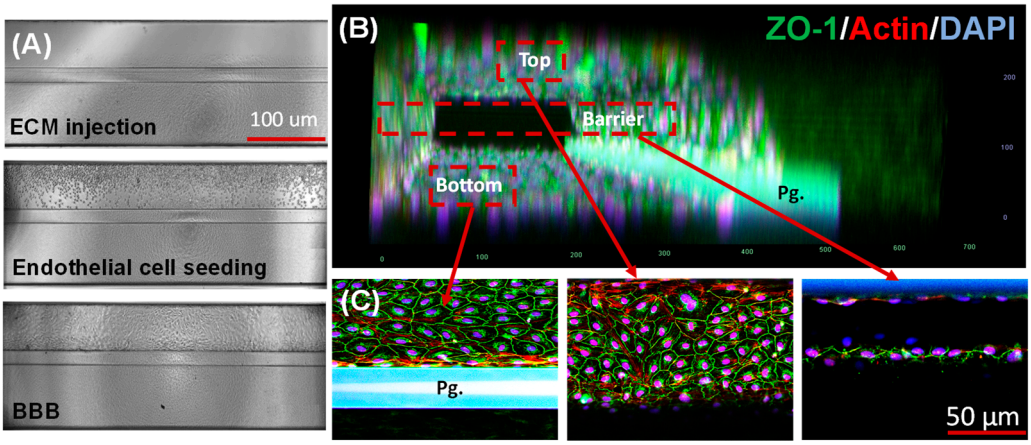

Figure 2. Perfused microvessels of endothelial cells in the microfluidic device. (**A**) The representative phase-contrast images of the BBB formation, (**B**) 3D construction of a confocal image showing a perfused endothelial microvessel with the lumen, the phase guide, and the ECM channel. (**C**) Immunostaining of an endothelial microvessel expressing the tight junction marker, ZO-1 (green), red-phalloidin stain for actin filaments, and DAPI (blue) stain for nuclei. All the images were acquired from the 8-day-old culture using a two-photon confocal microscope (ZEISS Multiphoton LSM 710) equipped with ZEN Blue software (Version 3.6, Carl Zeiss Microscopy GmbH).

Figure 2B shows a 3D reconstruction of a confocal image showing endothelial tubule formation featuring a top, middle, and bottom. Endothelial cell immunostaining showed the robust expression of ZO-1 (green) in cell margins which is characteristic of the BBB (Figure 2C). In addition to ZO-1 staining, we observed a distribution of actin filament (red) throughout the vascular bed and especially along the barrier. Figure 2C also shows the middle section of the BBB, showing the formation of a tight junction against the ECM, maintaining the barrier function without any physical membrane.

3.2. Barrier Formation Characterization

The barrier integrity of the BBB in the microfluidic device was determined by perfusing the media channels with fluorescein isothiocyanate FITC-dextran (MW: 40 kDa). The

permeability of the dye from the endothelial lumen into the adjacent ECM channels was monitored by the acquisition of fluorescent images using the time-lapse function with the stage incubator (Figure 3A). In the chips with an engineered BBB, but without the induction of $A\beta_{1–42}$ solution, a significant amount of the dye was found within the lumen (Figure 3A), and the average apparent permeability ($\boldsymbol{P}_{app}$) was 2.01×10^{-3} (Figure 3B). The chips without BBB (ECM only) and chips with BBB but induced with the $A\beta_{1–42}$ solution demonstrated significant diffusion of the dye into the adjacent ECM channel (Figure 3A), and the $\boldsymbol{P}_{app}$ values were 6.72×10^{-3}, 3.52×10^{-3}, 5.62×10^{-3}, and 5.89×10^{-3}, respectively (Figure 3B).

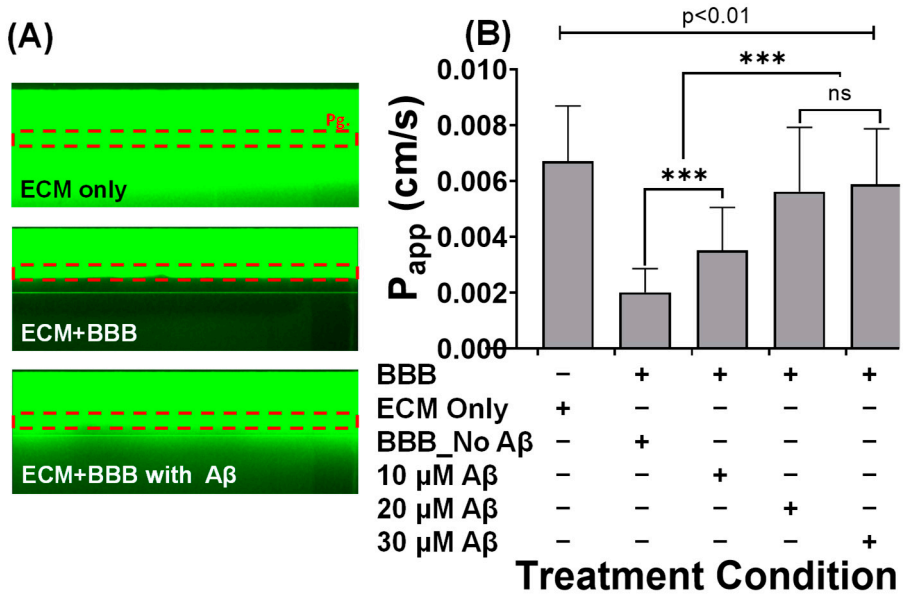

Figure 3. Characterization of the barrier formation in microfluidics. (**A**) Distributions of FITC dextran in the endothelial microvessel. Images were acquired in the absence of the BBB (ECM only, top), a leak-tight barrier (BBB without $A\beta_{1–42}$, middle), and a leaky barrier (BBB with $A\beta_{1–42}$, bottom). (**B**) Apparent permeability for assessing barrier function (for FITC-dextran, 40 kDa) at different time points for endothelial cells cultured under perfusion in the microfluidic device. Error bars show the standard deviation of the mean. The value represents the mean ± SD of two independent experiments with two replicates for each treatment condition. ns not significant and *** indicates $p < 0.0001$ compared with control (BBB_No Aβ) unless otherwise stated.

When the $\boldsymbol{P}_{app}$ values in the BBB with or without $A\beta_{1–42}$ are compared, it is clear that Aβ induced a 1.75-fold (10 μM), 2.79-fold (20 μM), and 2.93-fold (30 μM) increase in FITC permeability in the ECM (Figure 3B). However, ECM only showed a 3.34-fold increase in $\boldsymbol{P}_{app}$ value when compared with the BBB without $A\beta_{1–42}$ induction. When ECM only is compared with the highest concentration of $A\beta_{1–42}$ (30 μM), the permeability can be seen to have experienced a 1.14-fold increase. Although the $A\beta_{1–42}$ caused damage to the BBB, the presence of endothelial cells provided an additional barrier (Figure 3B).

3.3. $A\beta_{1–42}$ Treatment and Associated Tight Junction Behavior

It is important to note that, in this study, we analyzed only ZO-1 expression. While claudin-5 and occludin are critical components of tight junctions, ZO-1's multifaceted role as a scaffolding protein, a regulator of barrier function, and a mediator of signaling pathways makes it particularly important for tight junction expression. Its interactions with other tight junction proteins contribute to the overall integrity and functionality of tight junction complexes. We treated the BBB layer with four concentrations (0 μM, 10 μM, 20 μM, and 30 μM) of $A\beta_{1–42}$ to evaluate their impact on the BBB; we also treated the ECM-only channel without the BBB layer with a 20 μM $A\beta_{1–42}$ concentration to quantify the penetration of Aβ into the brain lane (Figure 4). Endothelial cells challenged with different

concentrations of $A\beta_{1–42}$ oligomer solutions for 48 h displayed an altered plasma membrane morphology of ZO-1 with non-specific staining for $A\beta_{1–42}$ (Figure 4A). Quantification of $A\beta_{1–42}$ migration and BBB formation and disruption were based on immunocytochemistry staining (Figure 4). The results were compared with the control (BBB model with no exposure to $A\beta_{1–42}$) (Figure 4). When the chip with ECM only was treated with 20 µM of $A\beta_{1–42}$, there was an increased $A\beta_{1–42}$ intensity in the ECM channels in comparison with the 10 µM ($p = 0.0432$), 20 µM ($p = 0.0331$), and 30 µM ($p = 0.0219$) $A\beta_{1–42}$ treatment (Figure 4B,C). The lowest $A\beta_{1–42}$ intensity in the ECM channels with BBB was found under the 30 µM condition in comparison with the 20 µM ($p = 0.4852$) and 10 µM ($p = 0.0412$) treatments (Figure 4B,C). As expected, we observed that Aβ is associated with a higher ECM penetration if there is no BBB in the chip (ECM only) (Figure 4C).

In all conditions, $A\beta_{1–42}$ and ZO-1 expression at the barrier were quantified. The increase in $A\beta_{1–42}$ intensity on the barrier of the endothelial tubule was associated with an increase in the concentration gradient of $A\beta_{1–42}$ (Figure 4D). $A\beta_{1–42}$ deposition on the barrier was compared, and the 30 µM treatment displayed the highest $A\beta_{1–42}$ intensity in comparison with the 20 µM ($p = 0.2747$), 10 µM ($p = 0.0006$), ECM only + 20 µM ($p = 0.0229$), and BBB-No Aβ conditions ($p = 0.0002$) (Figure 4D). There was no significant difference in $A\beta_{1–42}$ intensity between ECM only treated with Aβ 20 µM and the BBB layer treated with Aβ 20 µM ($p = 2107$). Our analysis shows that the ZO-1 intensity obtained at the barrier was higher in the BBB-No Aβ treatment in comparison with the 10 µM Aβ ($p = 0.0013$), 20 µM Aβ ($p = 0.0024$), and 30 µM Aβ ($p = 0.0104$) conditions (Figure 4E). ZO-1 staining did not reveal any significant differences between the 10 µM and 20 µM ($p = 0.0921$) treatmenets or between the 10 µM and 30 µM ($p = 0.2944$) treatments (Figure 4E).

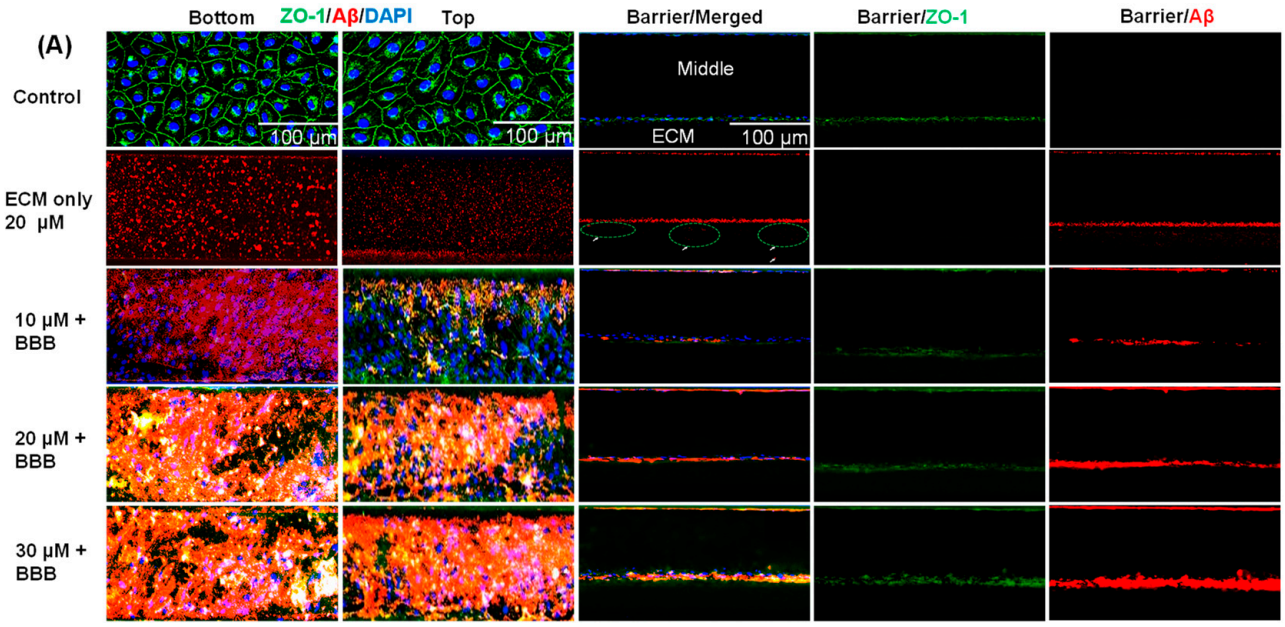

Figure 4. *Cont.*

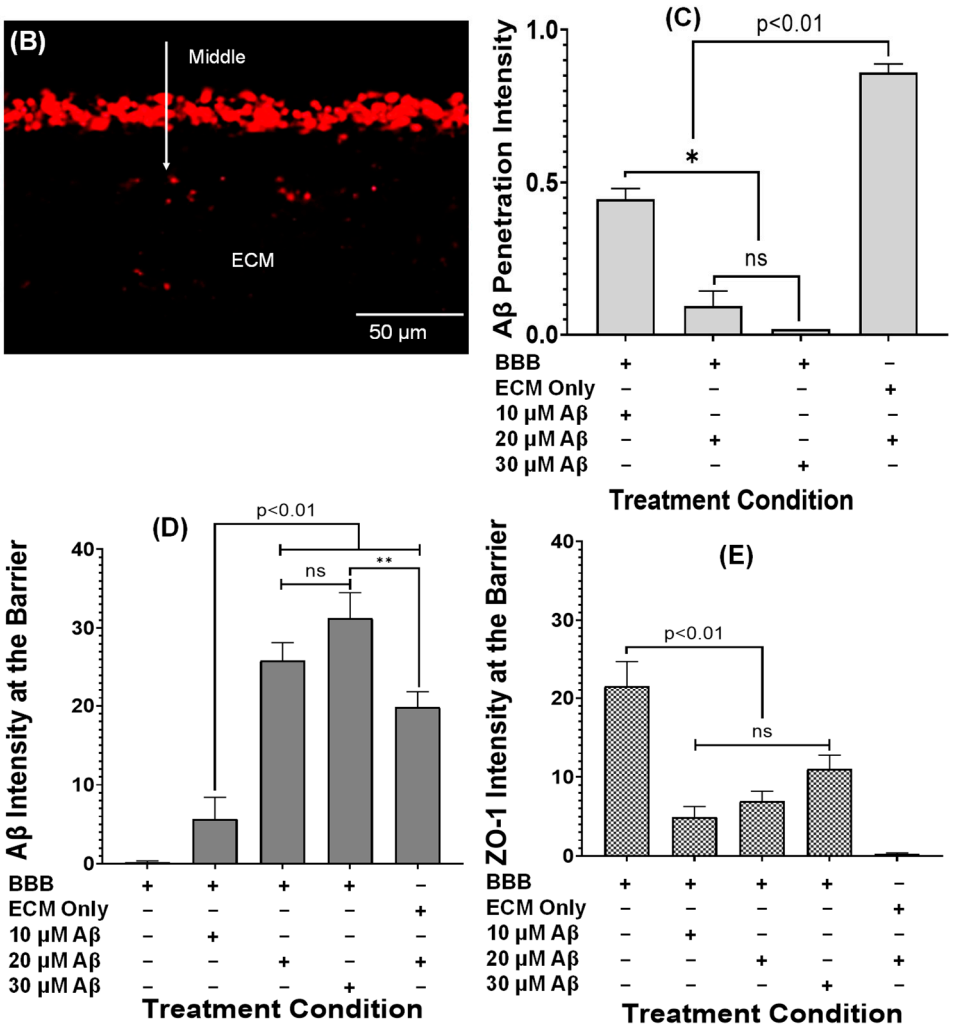

Figure 4. (**A**) Representative immunofluorescence images of 5 days of culture in a microfluidic device that were exposed to nothing (control) or $A\beta_{1–42}$ (10 µM, 20 µM, and 30 µM) for 48 h are shown (n = 2). They display the blood lane stained images of tight junction (ZO-1, green), amyloid beta ($A\beta_{1–42,}$ red), and nucleus (Hoechst, blue). The arrowheads indicate $A\beta_{1–42}$ that has penetrated the ECM in a chip without a barrier (Figure A-, ECM only 20 µM). (**B**) Representative image depicting penetration of $A\beta_{1–42}$ into the ECM channel in the absence of an endothelial barrier (ECM only 20 µM). (**C**) Quantification of the average intensity of $A\beta_{1–42}$ penetrated the ECM channel after 48 h. ECM only treated with 20 µM of $A\beta_{1–42}$ is the control for this figure. (**D**,**E**) $A\beta_{1–42}$ and ZO-1 quantification at the barrier at different concentrations using the same image threshold. The value represents the mean ± SD from two independent experiments with two replicates for each treatment condition. ns not significant, * indicates $p < 0.05$ and ** indicates $p < 0.01$ compared with one another unless otherwise stated. All conditions were compared to one another.

3.4. Effect of $A\beta_{1–42}$ on Endothelial Cell Viability

We quantified the effects of $A\beta_{1–42}$ on endothelial cell viability after 48 h of incubation (Figure 5). The cell viability assessment using confocal images of live/dead assay demonstrated a dose-dependent decrease in endothelial cell viability, accompanied by significant cell death (Figure 5A,B), with an estimated IC50 within 5.29 ± 7. When compared with the BBB-No Aβ (CTL; 76.9%, $p < 0.001$), exposure of $A\beta_{1–42}$ at 10 µM, 20 µM, and 30 µM to the blood lane significantly reduced the viability of endothelial cells by 59.1% ($p = 0.0030$), 40.8% ($p = 0.0030$), and 39.4% ($p = 0.0011$), respectively (Figure 5B). However, when the concentration gradient was compared to the viability, 20 µM and 30 µM were found to be comparable ($p = 0.9698$) but significantly lower than 10 µM (Figure 5, $p = 0.0020$).

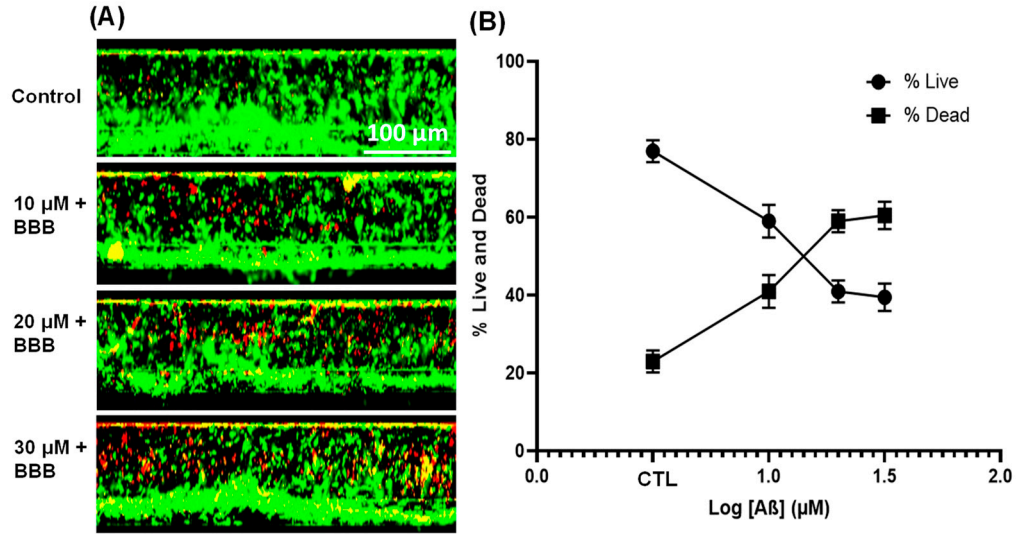

Figure 5. Cell viability assay of endothelial cells seeded on the two-lane microfluidics. (**A**) A representative series of confocal microscopy images depicting live/dead staining of endothelial tubules in microfluidic channels. Green fluorescence indicates live cells and red fluorescence indicates dead cells. (**B**) Percentage of live/dead 48 h following treatment with amyloid beta ($A\beta_{1–42}$). All data represent average viability measured within the top and bottom layers of the endothelial tubule. The value represents the mean ± SD for two independent experiments (n = 2 for each treatment condition).

4. Discussion

In this study, we present the creation of a high-throughput microfluidic device based on an in vitro model of the human blood–brain barrier (BBB) [21,29]. The patterning of ECM is made possible by the surface tension of the microfluidic platform. A BBB microvessel forms in the perfusion channel next to the ECM. The technique enables fluid-phase sampling of molecules that flow through the endothelium and extracellular matrix layers, allowing fluid to flow through BBB microvessels without the need for artificial membranes. We demonstrate that the model is sensitive to variations in Aβ concentrations. The focus of the paper is to investigate the transportation of Aβ oligomers across the blood–brain barrier (BBB), specifically examining Aβ accumulation and penetration at the BBB. This study has the potential to pave the way for future research to explore the role of Aβ transporters such as RAGE and LRP1 in mediating Aβ transport across the BBB. It is worth noting that the cells utilized in this model are immortalized, they may not have the same phenotype as BBB cells found in native cells. As a result, patient outcomes from this model might not be applicable directly. Nonetheless, regardless of the passage number, it has been demonstrated that the endothelial cell line in this investigation expresses tight junctional markers and forms BBB [30–34].

This paper examined the effect of $A\beta_{1–42}$ oligomer on the BBB grown on a membrane-free microfluidics device. We investigated (1) the integrity of the BBB, (2) the expression of ZO-1 tight junctional protein, and (3) cell viability before and after exposure to $A\beta_{1–42}$ solutions. In the microfluidic device, the endothelial layer formed the 3D tubular structure against the membrane-free ECM, which provides a physiologically relevant exposure route for $A\beta_{1–42}$. To determine the barrier integrity of the BBB, FITC was infused into the BBB cultures within the microfluidic device. Time-lapse photography was used to track FITC penetration in the ECM lane, and the apparent permeability ($\boldsymbol{P}_{app}$) was estimated. The same method was applied to determine $\boldsymbol{P}_{app}$ in chips that had or did not have an $A\beta_{1–42}$-treated endothelial microvessel. Our findings suggest that FITC diffuses through the ECM to the same degree whether the barrier is absent or the BBB has been modified with Aβ. The results demonstrate the increase in FITC permeability across the BBB with the increase in $A\beta_{1–42}$ concentrations (Figure 3).

Interestingly, we observed that an increase in $A\beta_{1–42}$ concentration was associated with an increase in the intensity of ZO-1 (Figure 4D,E). We believe that, when endothelial cells were treated with 20–30 μM $A\beta_{1–42}$, Aβ was accumulated on the wall of ECs against the ECM and formed cell–Aβ matrix aggregates, eventually forming the aggregate of dysfunctional BBB (Figure 6). It seems as though the complex cell–Aβ matrix does not allow Aβ penetration into the brain parenchyma (ECM channel/brain lane), with the Aβ intensity in the ECM decreasing with increasing Aβ concentrations (Figure 4C). On the other hand, when endothelial cells were treated with a lower concentration such as 10 μM $A\beta_{1–42}$, only a few locations showed cell–Aβ matrix aggregates bound, and cells maintained their homeostasis (Figure 4A,C). It is interesting to note that Aβ mimicked CAA pathogenesis by depositing on the wall of BBB against the ECM rather than passing through the compromised BBB into the brain lane. We believe that this will be the initial stage of Aβ accumulation on the BBB. Whether the aggregate of the cell–Aβ matrix complex structure will experience a reduction over time to allow the transport of $A\beta_{1–42}$ into the brain region has not been investigated. Investigating if Aβ transporter expression occurs on the ECs of our model will be necessary for future research.

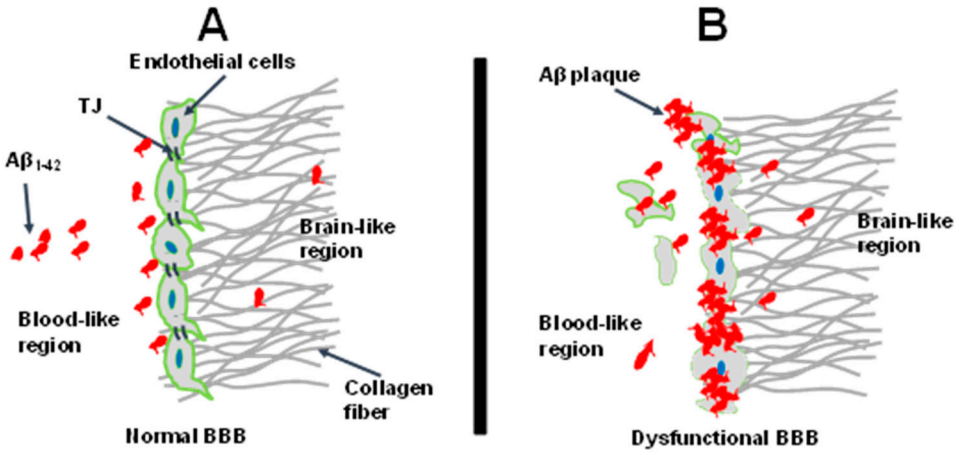

Figure 6. Schematic illustration of amyloid beta (Aβ) plaque aggregation with endothelial cells in the microfluidic device. Research rationale. (**A**): fully developed and functionally engineered BBB was challenged with different concentrations of $A\beta_{1–42}$. (**B**): Aβ accumulates on the endothelial cells and forms cell–Aβ aggregates, eventually forming the thicker dysfunctional BBB. At this stage (**B**), the higher concentrations (20 μM and 30 μM) of Aβ produce a higher Aβ–cell aggregate that may diffuse into the brain region in a small amount. A low concentration such as 10 μM forms fewer aggregates with the cells, allowing individual oligomers to penetrate the barrier and reach the brain-like region. However, the Aβ–cells 3D complex structures at the barrier do not deter the permeability of FITC through the broken BBB and endothelial cells.

It has been reported that Aβ causes damage to TJs and directly impairs BBB integrity, confirming the relationship between Aβ and AD [35,36]. Using a transwell assay technique, human brain endothelial cells (hCMEC/D3) have been used as a BBB model and treated to 0–40 μM of Aβs. The concentration of Aβs has been shown to increase the penetration ability of FITC-dextran: 40 μM of Aβs has been shown to produce the highest permeability when compared to the control of 0 μM, while 5 μM has been found to produce a relatively small change [37]. We also confirmed that a low concentration of 10 μM and a higher concentration of 30 μM of $A\beta_{1–42}$ for 48 h also induced structural damage in TJ (Figure 4A, $p < 0.001$). The FITC-dextran perfusion assay with microfluidic technology demonstrated increased perfusion with $A\beta_{1–42}$ in a concentration-dependent manner (Figure 3, $p < 0.001$), suggesting that $A\beta_{1–42}$ alters TJ architecture and digests BBB integrity [36,37]. Significant differences in the perfusion of FITC-dextran were found between the engineered BBB treated with $A\beta_{1–42}$ and the control (untreated), highlighting a possible neurotoxic effect of $A\beta_{1–42}$.

Of note is the fact that the concentrations of $A\beta_{1–42}$ used in this study are higher than the physiological concentration of $A\beta_{40/42}$ in the blood [38]. However, we did not observe any defined mechanism of $A\beta_{1–42}$ localization. There is published evidence that when the endothelial cells are impaired they release proinflammatory cytokines, increasing neuroinflammation and secondary alteration, ultimately resulting in the disruption of the TJ and BBB [39]. The cell stretching due to accumulation of $A\beta_{1–42}$ may be due to impaired cell cytoskeleton, retard movement of the endothelial cells, and cause their death [40]. Aβ affects endothelial cells (ECs) in the brain microvasculature directly or indirectly by changing TJP distribution, encouraging EC mortality, increasing oxidative stress, and stimulating glial cell production of pro-inflammatory cytokines [38,41]. In CAA mice models and human patients, Aβ buildup has a deleterious effect on brain artery walls, resulting in BBB disruption and possible bleeding [42,43]. Research conducted in vitro has demonstrated that exposure to Aβ leads to actin organization disruption and death in ECs [40]. Moreover, matrix metalloproteinases (MMPs) are expressed at higher levels while TJ protein expression is diminished in CAA patients and mice overexpressing amyloid precursor protein (APP) [43]. Additionally, the presence of Aβ inhibits the interaction between heat shock protein 90 and endothelial nitric oxide synthase [44] and encourages the development of von Willebrand factor (VWF) fibrils, which are linked to thrombogenic and inflammatory reactions in brain arteries [45]. These published results emphasize the harmful effects of Aβ deposition on artery walls, including the disruption of ECs and a weakened BBB. The loss of vascular control may be caused by any one of the above processes. We chose the most critical factors for in vitro modeling, including (1) endothelial cell barrier formation, (2) perfusion in a high throughput manner, and (3) membrane-free layer. This allowed the study of direct interactions between amyloid beta and the barrier layer such as accumulation of amyloid beta oligomer. Subsequent investigations with more complex vascular cells such as astrocytes and pericytes may provide better insights into amyloid beta interactions with the BBB.

5. Conclusions

We effectively created a three-dimensional perfused BBB-on-a-chip and studied Aβ trafficking. The resulting vascular network displayed lumens and BBB features. We examined the effect of $A\beta_{1–42}$ on the physiological function of BBB in a perfusion channel. Our findings demonstrate a pronounced accumulation of $A\beta_{1–42}$ oligomers at the BBB, resulting in the disruption of tight junctions and subsequent leakage evidenced by barrier integrity assay. We confirmed the formation of tubules in the microfluidic chips and that TJ plays an important role in BBB permeability.

Author Contributions: Methodology, S.C.U. and Y.Y.; Validation, Y.Y.; Formal analysis, S.C.U., C.J.B. and Y.Y.; Investigation, Y.Y.; Resources, Y.Y.; Data curation, S.C.U.; Writing—original draft, S.C.U.; Writing—review & editing, B.E.C., Y.L., S.S.K., D.Y.K., D.T.L., J.-M.L. and Y.Y.; Supervision, Y.Y.; Funding acquisition, Y.Y. All authors have read and agreed to the published version of the manuscript.

Funding: This work was supported by the National Science Foundation (Award No. 2100987, 2315654, and 2133630), Cure Alzheimer's Fund (#A069137), and the National Institutes of Health (Award No. 1SC1NS122448, and 1R01AG082093-01).

Institutional Review Board Statement: Not applicable.

Informed Consent Statement: Not applicable.

Data Availability Statement: Data are contained within the article.

Conflicts of Interest: The authors declare no conflict of interest.

References

1. Dobbing, J. The Blood-Brain Barrier. *Dev. Med. Child Neurol.* **1961**, *3*, 610–612. [CrossRef]
2. Liu, L.; Koo, Y.; Akwitti, C.; Russell, T.; Gay, E.; Laskowitz, D.T.; Yun, Y. Three-dimensional (3D) brain microphysiological system for organophosphates and neurochemical agent toxicity screening. *PLoS ONE* **2019**, *14*, e0224657. [CrossRef]

3. Abbott, N.J.; Patabendige, A.A.K.; Dolman, D.E.M.; Yusof, S.R.; Begley, D.J. Structure and function of the blood-brain barrier. *Neurobiol. Dis.* **2010**, *37*, 13–25. [CrossRef]
4. Wevers, N.R.; de Vries, H.E. Morphogens and blood-brain barrier function in health and disease. *Tissue Barriers* **2016**, *4*, e1090524. [CrossRef] [PubMed]
5. Pardridge, W.M. Drug transport across the blood-brain barrier. *J. Cereb. Blood Flow Metab.* **2012**, *32*, 1959–1972. [CrossRef]
6. Murphy, M.P.; LeVine, H., 3rd. Alzheimer's disease and the amyloid-β peptide. *J. Alzheimer's Dis.* **2010**, *19*, 311–323. [CrossRef]
7. Wan, W.; Cao, L.; Liu, L.; Zhang, C.; Kalionis, B.; Tai, X.; Li, Y.; Xiantao, T. Aβ1–42 oligomer-induced leakage in an in vitro blood-brain barrier model is associated with up-regulation of RAGE and metalloproteinases, and down-regulation of tight junction scaffold proteins. *J. Neurochem.* **2015**, *134*, 382–393. [CrossRef]
8. Zlokovic, B.V.; Gottesman, R.F.; Bernstein, K.E.; Seshadri, S.; McKee, A.; Snyder, H.; Greenberg, S.M.; Yaffe, K.; Schaffer, C.B.; Yuan, C.; et al. Vascular contributions to cognitive impairment and dementia (VCID): A report from the 2018 National Heart, Lung, and Blood Institute and National Institute of Neurological Disorders and Stroke Workshop. *Alzheimer's Dement.* **2020**, *16*, 1714–1733. [CrossRef]
9. Biffi, A.; Greenberg, S.M. Cerebral amyloid angiopathy: A systematic review. *J. Clin. Neurol.* **2011**, *7*, 1–9. [CrossRef]
10. Bilodeau, P.A.; Dickson, J.R.; Kozberg, M.G. The Impact of Anti-Amyloid Immunotherapies on Stroke Care. *J. Clin. Med.* **2024**, *13*, 1245. [CrossRef] [PubMed]
11. Wan, W.; Chen, H.; Li, Y. The potential mechanisms of A beta-receptor for advanced glycation end-products interaction disrupting tight junctions of the blood-brain barrier in Alzheimer's disease. *Int. J. Neurosci.* **2014**, *124*, 75–81. [CrossRef] [PubMed]
12. Zhang, Y.; Chen, H.; Li, R.; Sterling, K.; Song, W. Amyloid β-based therapy for Alzheimer's disease: Challenges, successes and future. *Signal Transduct. Target. Ther.* **2023**, *8*, 248. [CrossRef] [PubMed]
13. Yang, Y.; Rosenberg, G.A. MMP-Mediated Disruption of Claudin-5 in the Blood–Brain Barrier of Rat Brain After Cerebral Ischemia. *Methods Mol. Biol.* **2011**, *762*, 333–345. [CrossRef] [PubMed]
14. Wevers, N.R.; de Vries, H.E. Modeling ischemic stroke in a triculture neurovascular unit on-a-chip. *Fluids Barriers CNS* **2021**, *18*, 1–18. [CrossRef] [PubMed]
15. Abbott, N.J.; Hughes, C.C.W.; Revest, P.A.; Greenwood, J. Development and characterisation of a rat brain capillary endothelial culture: Towards an in vitro blood-brain barrier. *J. Cell Sci.* **1992**, *103*, 23–37. [CrossRef] [PubMed]
16. Biegel, D.; Pachter, J.S. Growth of brain microvessel endothelial cells on collagen gels: Applications to the study of blood-brain barrier physiology and CNS inflammation. *Vitr. Cell Dev Biol Anim.* **1994**, *30A*, 581–588. [CrossRef]
17. He, Y.; Yao, Y.; Tsirka, S.E.; Cao, Y. Cell-Culture Models of the Blood–Brain Barrier. *Stroke* **2014**, *45*, 2514–2526. [CrossRef] [PubMed]
18. Wolff, A.; Antfolk, M.; Brodin, B.; Tenje, M. In Vitro Blood-Brain Barrier Models-An Overview of Established Models and New Microfluidic Approaches. *J. Pharm. Sci.* **2015**, *101*, 2727–2746. [CrossRef]
19. Li, Y.; Li, D.; Zhao, P.; Nandakumar, K.; Wang, L.; Song, Y. Microfluidics-based systems in diagnosis of Alzheimer's disease and biomimetic modeling. *Micromachines* **2020**, *11*, 787. [CrossRef]
20. Prabhakarpandian, B.; Shen, M.-C.; Nichols, J.B.; Mills, I.R.; Sidoryk-Wegrzynowicz, M.; Aschner, M.; Pant, K. SyM-BBB: A microfluidic blood brain barrier model. *Lab Chip* **2013**, *13*, 1093–1101. [CrossRef]
21. Koo, Y.; Hawkins, B.T.; Yun, Y. Three-dimensional (3D) tetra-culture brain on chip platform for organophosphate toxicity screening. *Sci. Rep.* **2018**, *8*, 2841. [CrossRef] [PubMed]
22. Russell, T.; Dirar, Q.; Li, Y.; Chiang, C.; Laskowitz, D.T.; Yun, Y. Cortical Spheroid on Perfusable Microvascular Network in a Microfluidic Device. *PLoS ONE* **2023**, *18*, e0288025. [CrossRef] [PubMed]
23. Wevers, N.R.; Kasi, D.G.; Gray, T.; Wilschut, K.J.; Smith, B.; van Vught, R.; Shimizu, F.; Sano, Y.; Kanda, T.; Marsh, G.; et al. A perfused human blood-brain barrier on-a-chip for high-throughput assessment of barrier function and antibody transport. *Fluids Barriers CNS* **2018**, *15*, 23. [CrossRef] [PubMed]
24. Bonanini, F.; Kurek, D.; Previdi, S.; Nicolas, A.; Hendriks, D.; de Ruiter, S.; Meyer, M.; Cabrer, M.C.; Dinkelberg, R.; García, S.B.; et al. In vitro grafting of hepatic spheroids and organoids on a microfluidic vascular bed. *Angiogenesis* **2022**, *25*, 455–470. [CrossRef] [PubMed]
25. Stine, W.B.; Dahlgren, K.N.; Krafft, G.A.; LaDu, M.J. In vitro characterization of conditions for amyloid-β peptide oligomerization and fibrillogenesis. *J. Biol. Chem.* **2003**, *278*, 11612–11622. [CrossRef] [PubMed]
26. Fa, M.; Orozco, I.J.; Francis, Y.I.; Saeed, F.; Gong, Y.; Arancio, O. Preparation of oligomeric β-amyloid1–42 and induction of synaptic plasticity impairment on hippocampal slices. *J. Vis. Exp.* **2010**, *41*, e1884. [CrossRef] [PubMed]
27. Soragni, C.; Vergroesen, T.; Hettema, N.; Rabussier, G.; Lanz, H.L.; Trietsch, S.J.; de Windt, L.J.; Ng, C.P. Quantify permeability using on-a-chip models in high-throughput applications. *STAR Protoc.* **2023**, *4*, 102051. [CrossRef] [PubMed]
28. Nicolas, A.; Trietch, S.J. High throughput transepithelial electrical resistance (TEER) measurements on perfused membrane-free epithelia. *Lab Chip* **2021**, *21*, 1676–1685. [CrossRef]
29. Liu, L.; Koo, Y.; Russell, T.; Gay, E.; Li, Y.; Yun, Y. Three-dimensional brain-on-chip model using human iPSC-derived GABAergic neurons and astrocytes: Butyrylcholinesterase posttreatment for acute malathion exposure. *PLoS ONE* **2020**, *15*, e0230335. [CrossRef]

30. Bok, J.-S.; Byun, S.-H.; Park, B.-W.; Kang, Y.-H.; Lee, S.-L.; Rho, G.-J.; Hwang, S.-C.; Woo, D.K.; Lee, H.-J.; Byun, J.-H. The role of human umbilical vein endothelial cells in osteogenic differentiation of dental follicle-derived stem cells in in vitro co-cultures. *Int. J. Med. Sci.* **2018**, *15*, 1160–1170. [CrossRef]
31. Bachetti, T.; Morbidelli, L. Endothelial cells in culture: A model for studying vascular functions. *Pharmacol. Res.* **2000**, *42*, 9–19. [CrossRef]
32. Medina-Leyte, D.J.; Domínguez-Pérez, M.; Mercado, I.; Villarreal-Molina, M.T.; Jacobo-Albavera, L. Use of Human Umbilical Vein Endothelial Cells (HUVEC) as a Model to Study Cardiovascular Disease: A Review. *Appl. Sci.* **2020**, *10*, 938. [CrossRef]
33. Santaterra, V.A.G.; Fiusa, M.M.L.; Hounkpe, B.W.; Chenou, F.; Tonasse, W.V.; da Costa, L.N.G.; Garcia-Weber, D.; Domingos, I.d.F.; de Lima, F.; Borba-Junior, I.T.; et al. Endothelial Barrier Integrity Is Disrupted In Vitro by Heme and by Serum From Sickle Cell Disease Patients. *Front. Immunol.* **2020**, *11*, 535147. [CrossRef] [PubMed]
34. Bartosova, M.; Ridinger, D.; Marinovic, I.; Heigwer, J.; Zhang, C.; Levai, E.; Westhoff, J.H.; Schaefer, F.; Terjung, S.; Hildenbrand, G.; et al. An experimental workflow for studying barrier integrity, permeability, and tight junction composition and localization in a single endothelial cell monolayer: Proof of concept. *Int. J. Mol. Sci.* **2021**, *22*, 8178. [CrossRef] [PubMed]
35. Claudio, L. Ultrastructural features of the blood-brain barrier in biopsy tissue from Alzheimer's disease patients. *Acta Neuropathol.* **1996**, *91*, 6–14. [CrossRef] [PubMed]
36. Marco, S.; Skaper, S.D. Amyloid β-peptide1–42 alters tight junction protein distribution and expression in brain microvessel endothelial cells. *Neurosci. Lett.* **2006**, *401*, 219–224. [CrossRef] [PubMed]
37. Li, Y.; Ni, N.; Lee, M.; Wei, W.; Andrikopoulos, N.; Kakinen, A.; Davis, T.P.; Song, Y.; Ding, F.; Leong, D.T.; et al. Endothelial leakiness elicited by amyloid protein aggregation. *Nat. Commun.* **2024**, *15*, 613. [CrossRef] [PubMed]
38. Tarafdar, A.; Wolska, N.; Krisp, C.; Schlüter, H.; Pula, G. The amyloid peptide β disrupts intercellular junctions and increases endothelial permeability in a NADPH oxidase 1-dependent manner. *Redox Biol.* **2022**, *52*, 102287. [CrossRef] [PubMed]
39. Pober, J.S.; Sessa, W.C. Evolving functions of endothelial cells in inflammation. *Nat. Rev. Immunol.* **2007**, *7*, 803–815. [CrossRef]
40. Take, Y.; Chikai, Y.; Shimamori, K.; Kuragano, M.; Kurita, H.; Tokuraku, K. Amyloid β aggregation induces human brain microvascular endothelial cell death with abnormal actin organization. *Biochem. Biophys. Rep.* **2021**, *29*, 101189. [CrossRef]
41. Zenaro, E.; Piacentino, G.; Constantin, G.; Brito, M. The blood-brain barrier in Alzheimer's disease. *Neurobiol. Dis.* **2017**, *107*, 41–56. [CrossRef]
42. Fisher, M.; Vasilevko, V.; Passos, G.F.; Ventura, C.; Quiring, D.; Cribbs, D.H. Therapeutic modulation of cerebral microhemorrhage in a mouse model of cerebral amyloid angiopathy. *Stroke* **2011**, *42*, 3300–3303. [CrossRef] [PubMed]
43. Hartz, A.M.; Bauer, B.; Soldner, E.L.; Wolf, A.; Boy, S.; Backhaus, R.; Mihaljevic, I.; Bogdahn, U.; Klünemann, H.H.; Schuierer, G.; et al. Amyloid-β contributes to blood-brain barrier leakage in transgenic human amyloid precursor protein mice and in humans with cerebral amyloid angiopathy. *Stroke* **2012**, *43*, 514–523. [CrossRef] [PubMed]
44. Lamoke, F.; Mazzone, V.; Persichini, T.; Maraschi, A.; Harris, M.B.; Venema, R.C.; Colasanti, M.; Gliozzi, M.; Muscoli, C.; Bartoli, M.; et al. Amyloid β peptide-induced inhibition of endothelial nitric oxide production involves oxidative stress-mediated constitutive eNOS/HSP90 interaction and disruption of agonist-mediated Akt activation. *J. Neuroinflammation* **2015**, *12*, 84. [CrossRef] [PubMed]
45. Shulyatnikova, T.; Hayden, M.R. Why Are Perivascular Spaces Important? *Medicina* **2023**, *59*, 917. [CrossRef] [PubMed]